

Synchrotron Self Absorption in GRB Afterglow

Jonathan Granot, Tsvi Piran and Re'em Sari

Racah Institute, Hebrew University, Jerusalem 91904, Israel

September 29, 2018

Abstract

GRB afterglow is reasonably described by synchrotron emission from relativistic blast waves at cosmological distances. We perform detailed calculations taking into account the effect of synchrotron self absorption. We consider emission from the whole region behind the shock front, and use the Blandford McKee self similar solution to describe the fluid behind the shock. We calculate the spectra and the observed image of a GRB afterglow near the self absorption frequency ν_a and derive an accurate expression for ν_a . We show that the image is rather homogeneous for $\nu < \nu_a$, as opposed to the bright ring at the outer edge and dim center, which appear at higher frequencies. We compare the spectra we obtain to radio observations of GRB970508. We combine the calculations of the spectra near the self absorption frequency with other parts of the spectra and obtain revised estimates for the physical parameters of the burst: $E_{52} = 0.53$, $\epsilon_e = 0.57$, $\epsilon_B = 0.0082$, $n_1 = 5.3$. These estimates are different by up to two orders of magnitude than the estimates based on an approximate spectrum.

1 Introduction

The detection of delayed x-ray, optical and radio emission following a GRB, known as GRB afterglow, is described reasonably well by emission from a spherical relativistic shell, decelerating upon collision with an ambient

medium (Waxman 1997a, Wijers, Rees & Mészáros 1997, Katz & Piran 1997, Sari, Piran & Narayan 1998). A relativistic blast wave expands through the ambient medium, continuously heating up fresh matter as it passes through the shock. In these models, the GRB afterglow is the result of synchrotron emission of the relativistic electrons of the heated matter.

Several recent works considered emission from various regions on or behind the shock front (Waxman 1997c, Sari 1998, Panaitescu & Mészáros 1998, Granot, Piran & Sari 1998 (GPS hereafter), Gruzinov & Waxman 1998). These authors considered the spectra near the peak frequency ν_m and found that exact calculations of the spectrum could differ by up to one order of magnitude from simpler estimates.

We consider emission from an adiabatic highly relativistic blast wave expanding into a cold and uniform medium. We consider the effect of the whole volume behind the shock front, the importance of which was stressed in GPS. The hydrodynamics is described by the Blandford McKee (1976 denoted BM hereafter) self similar solution. We consider synchrotron emission and we ignore Compton scattering and electron cooling. Similar to GPS, we consider several models for the evolution of the magnetic field.

Synchrotron self absorption becomes significant below a critical frequency ν_a called the self absorption frequency. We assume that $\nu_a \ll \nu_m$, where ν_m is the peak frequency, which is reasonable for the first few months after the burst. While the spectrum near ν_m was quite extensively studied, so far only order of magnitude estimates of the spectrum near the self absorption frequency ν_a were done.

For a system in which $\nu_a \ll \nu_m$, the spectrum, F_ν , is proportional to ν^2 for $\nu \ll \nu_a$, rather than the standard $\nu^{5/2}$, because almost all the low frequency radiation is emitted by electrons with a typical synchrotron frequency much higher than ν_a (Katz 1994). The spectra far above ν_a is proportional to $\nu^{1/3}$. In this paper we explore the spectra near ν_a , and find how the two asymptotic forms join together. An analysis of the spectra over a wider range of frequencies was made by Sari, Piran & Narayan (1998), and a detailed analysis of the spectra near the peak frequency, taking a full account of the BM solution, was made in GPS and Gruzinov & Waxman (1998).

The physical model is described in §2. In §3 we describe the computational formalism. The spectra for several magnetic field models and the observed image of a GRB afterglow at various frequencies are presented in §4. In §5 we compare the calculated spectra to radio observations of the

afterglow of GRB970508. When we use the modified calculations of the self absorption spectra and of the spectra around the peak (GPS) and the cooling frequency (Sari, Piran & Narayan 1998) we find new estimates of the parameters of GRB970508. These estimates are different by more than an order of magnitude than estimates based on a simpler broken power law spectra (Wijers & Galama 1998).

2 The Physical Model

The underlying model assumes an ultra-relativistic spherical blast wave expanding into a cold and uniform medium. The blast wave constantly heats fresh matter, and the observed afterglow is the result of synchrotron emission of the relativistic electrons of the heated matter. We consider an adiabatic evolution, where the fluid behind the shock is described by the BM self similar solution. It has been numerically verified that for an adiabatic evolution with general initial conditions the solution approaches the BM solution (Kobayashi, Piran & Sari 1998). The BM solution is expressed in terms of the similarity variable χ , which is defined by:

$$\chi \equiv 1 + 16\gamma_f^2 \left(\frac{R-r}{R} \right), \quad (1)$$

where R is the radius of the shock front, r is the distance of a point from the center of the burst and γ_f is the Lorentz factor of the matter just behind the shock. The BM solution is given by:

$$n' = 4\gamma_f n_0 \chi^{-5/4}, \quad \gamma = \gamma_f \chi^{-1/2}, \quad e' = 4n_0 m_p c^2 \gamma_f^2 \chi^{-17/12}, \quad (2)$$

where n' and e' are the number density and the energy density in the local frame, respectively, γ is the Lorentz factor of the bulk motion of the matter behind the shock, m_p is the mass of a proton and $n_0 = n_1 \times 1\text{cm}^{-3}$ is the proper number density of the unshocked ambient medium.

We consider three alternative models for the magnetic field: B , B_\perp and B_{rad} . B satisfies $e'_{B'} = \epsilon_B e'$ (i.e. equipartition) everywhere. For the two other magnetic field models we assume they acquire $e'_{B'} = \epsilon_B e'$ on the shock front, and from then on, evolve according to the “frozen field” approximation. This implies that the magnetic fields equal $B\chi^{3\delta/2}$, where $\delta = 7/18$ when the

magnetic field is in the radial direction (B_{rad}) and $\delta = -7/36$ when the magnetic field is perpendicular to the radial direction (B_{\perp}) (see GPS).

We assume that the energy of the electrons is everywhere a constant fraction of the internal energy: $e'_{el} = \epsilon_e e'$, and that the shock produces a power law electron distribution: $N(\gamma_e) = K \gamma_e^{-p}$ ¹ for $\gamma_e \geq \gamma_{min}$. We use $p = 2.5$ wherever a definite numerical value of p is needed. The constants K and γ_{min} in the electron distribution can be calculated from the number density and energy density:

$$\gamma_{min} = \left(\frac{p-2}{p-1} \right) \frac{\epsilon_e e'}{n' m_e c^2} \quad , \quad K = (p-1) n' \gamma_{min}^{p-1} . \quad (3)$$

We consider frequencies which are much lower than the typical synchrotron frequency $\nu \ll \nu_{syn}$, where the spectral power of an electron emitting synchrotron radiation can be approximated by:

$$P'_{\nu',e} \cong \frac{2^{5/3} \pi}{\Gamma(1/3)} \frac{q_e^3 B' \sin \alpha}{m_e c^2} \left(\frac{\nu'}{\nu'_{syn}} \right)^{1/3} \quad , \quad \nu'_{syn} \equiv \frac{3 \gamma_e^2 q_e B' \sin \alpha}{4 \pi m_e c} \quad , \quad (4)$$

(Rybicki & Lightman 1979) where Γ is the gamma function, B' is the magnetic field, m_e and q_e are the mass and the electric charge of the electron, respectively, and α is the angle between the directions of the electron's velocity and the magnetic field, in the local frame.

R_l and γ_l are the location of the shock and its Lorentz factor on this line of sight and R_l/γ_l is an estimate of the shell thickness in the local frame. The optical depth along the LOS can be approximated by $\alpha'_{\nu'} R_l/\gamma_l$ where the absorption coefficient $\alpha'_{\nu'}$ is taken at $y = \chi = 1$. The ‘‘back of the envelope’’ estimate for the self absorption frequency ν_0 is therefore the frequency which satisfies: $\alpha'_{\nu'_0} R_l/\gamma_l = 1$. ν_0 is given by:

$$\nu_0 = 4.24 \times 10^9 (1+z)^{-1} \left(\frac{p+2}{3p+2} \right)^{3/5} \frac{(p-1)^{8/5}}{(p-2)} \epsilon_e^{-1} \epsilon_B^{1/5} E_{52}^{1/5} n_1^{3/5} \text{Hz} \quad , \quad (5)$$

where z is the cosmological red shift and $E = E_{52} \times 10^{52}$ ergs is the total energy of the shell. We also define a ‘‘standard’’ flux density F_0 , which is an

¹for the energy of the electrons to remain finite we must have $p > 2$.

approximate expression for the flux density at the self absorption frequency. The peak flux and peak frequency can be approximated by:

$$F_m \equiv \frac{(1+z)}{3} \frac{n_1 R_l^3}{d_L^2} \left(\frac{\gamma P'_e}{\nu'_{syn}} \right) (y = \chi = 1) \quad , \quad \nu_m \equiv \nu_{syn}(\gamma_{min}, y = \chi = 1) \quad , \quad (6)$$

(see F_0 and ν_T in GPS) where $P'_e = (4/3)\sigma_T c \gamma_e^2 e'_B$ is the total emitted power of an extreme relativistic electron (Rybicki & Lightman 1979), σ_T is the Thomson cross section and $d_L = d_{L28} \times 10^{28} \text{cm}$ is the luminosity distance². Now we can define: $F_0 \equiv F_m(\nu_a/\nu_m)^{1/3}$:

$$F_0 = 1.31(1+z) \left(\frac{p+2}{3p+2} \right)^{1/5} \frac{(p-1)^{6/5}}{(p-2)} d_{L28}^{-2} \epsilon_e^{-1} \epsilon_B^{2/5} E_{52}^{9/10} n_1^{7/10} T_{days}^{1/2} \text{mJy} \quad , \quad (7)$$

where T_{days} is the observed time in days.

We express the observed frequency ν in units of ν_0 : $\nu \equiv \phi \nu_0$, thus introducing the dimensionless variable ϕ which we use to express our results.

3 The Formalism

We consider a system that is moving relativistically while emitting radiation, and obtain a formula for the flux density measured by a distant observer, allowing for self absorption. We denote quantities measured in the local rest frame of the matter with a prime, while quantities without a prime are measured in the observer frame.

The specific intensity I_ν (energy per unit time per unit area per unit frequency per unit solid angle) satisfies the radiative transfer equation:

$$\frac{dI_\nu}{ds} = j_\nu - \alpha_\nu I_\nu \quad , \quad (8)$$

where j_ν and α_ν are the emission coefficient and the absorption coefficient, respectively, and s is the distance along the beam. When self absorption becomes important the contribution to I_ν depends on the optical depth along the path within the emitting system and I_ν should be integrated separately for every trajectory.

²Here and latter we use a general cosmological model. For a given model we should substitute the appropriate expression for $d_L(1+z, H_0)$.

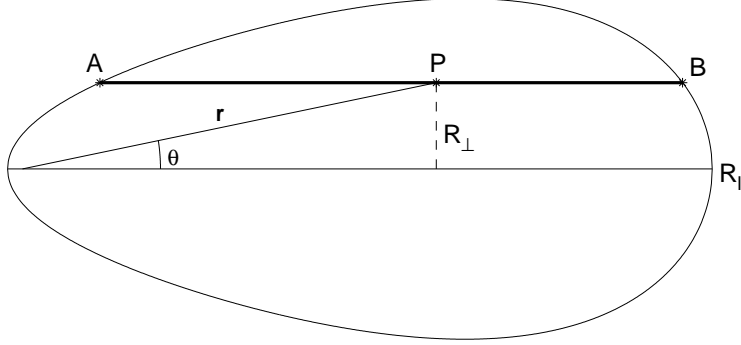


Figure 1: The egg-Shaped curve is the boundary of the region from which photons reach a distant observer simultaneously. The observer is located far to the right and the symmetry axis is the LOS from the source of the burst to the observer. The bold line represents the trajectory of a photon that reaches the observer. For a distant observer these trajectories are almost parallel to the LOS, and are therefore characterized by their distance R_{\perp} from the LOS. $I_{\nu} = 0$ at point A, and reaches its final value at point B. A photon emitted at a point P can be absorbed or cause stimulated emission at any point along the trajectory, until it passes the shock front at point B.

For the BM solution, the radius of the shock front and the Lorentz factor of the matter just behind the shock, on the LOS for a given observed time T , are given by:

$$\gamma_l \cong 3.65 E_{52}^{1/8} n_1^{-1/8} T_{days}^{-3/8} \quad , \quad R_l \cong 5.53 \times 10^{17} E_{52}^{1/4} n_1^{-1/4} T_{days}^{1/4} \text{cm} . \quad (9)$$

For a given observed time T , we use the coordinates y and χ , instead of the polar coordinates r and θ , where y is defined by $y \equiv R/R_l$. R is the radius of the shock front at the time t at which a photon must be emitted in order to reach the observer at the observed time T . A photon emitted at a location (r, θ) at a time t in the observer frame, reaches the observer at an observed time T given by:

$$T = t - \frac{r\mu}{c} \quad , \quad (10)$$

where $\mu \equiv \cos \theta$ (for more details on the coordinates, see GPS).

Since the observer is distant, the trajectory of a photon that reaches the observer is almost parallel to the LOS in the observer frame (see Figure 1).

We can therefore parameterize the various trajectories by their distance from the LOS. The distance R_{\perp} of a point from the LOS is given by:

$$R_{\perp} \equiv r \sin \theta \cong R_l y \sqrt{1 - \mu^2} \cong \frac{\sqrt{2} R_l}{4\gamma_l} \sqrt{y - \chi y^5} . \quad (11)$$

The maximal value of R_{\perp} is obtained for $\chi = 1$, $y = 5^{-1/4}$ and is given by:

$$R_{\perp, max} = 3.91 \times 10^{16} E_{52}^{1/8} n_1^{-1/8} T_{days}^{5/8} \text{ cm} , \quad (12)$$

We express R_{\perp} in units of $R_{\perp, max}$, introducing the dimensionless variable:

$$x \equiv \frac{R_{\perp}}{R_{\perp, max}} = \frac{5^{5/8}}{2} \sqrt{y - \chi y^5} . \quad (13)$$

In order to solve equation 8, explicit expressions for the absorption and the emission coefficients are needed. We consider an isotropic electron velocity distribution, and since $P'_{\nu', e} \propto \sin^{2/3} \alpha$ we use the averaged value $\langle \sin^{2/3} \alpha \rangle = \sqrt{\pi} \Gamma(1/3) / 5 \Gamma(5/6)$. The total power per unit volume per unit frequency in the local frame is given by:

$$P'_{\nu'} = \int_{\gamma_{min}}^{\infty} d\gamma_e N(\gamma_e) P'_{\nu', e} = \frac{64\pi^{13/6} 3^{2/3}}{5\Gamma(5/6)} \frac{(p-1)^{5/3}}{(3p-1)(p-2)^{2/3}} \frac{\epsilon_B^{1/3} \gamma_l n_0^{4/3} q_e^{8/3} \nu'^{1/3}}{m_p^{1/3} c y^{3/2} \chi^{29/18-\delta}} . \quad (14)$$

Assuming the emission and absorption are isotropic in the local rest frame of the matter, $j'_{\nu'} = P'_{\nu'} / 4\pi$ and the absorption coefficient is given by:

$$\alpha'_{\nu'} = \frac{(p+2)}{8\pi m_e \nu'^2} \int_{\gamma_{min}}^{\infty} d\gamma_e P'_{\nu', e}(\gamma_e) \frac{N(\gamma_e)}{\gamma_e} = \frac{8\pi^{7/6} 3^{2/3}}{5\Gamma(5/6)} \frac{(p+2)(p-1)^{8/3}}{(3p-2)(p-2)^{5/3}} \frac{\epsilon_b^{1/3} n_0^{4/3} q_e^{8/3}}{\epsilon_e^{5/3} m_p^{4/3} c \nu'^{5/3} \chi^{13/9-\delta}} , \quad (15)$$

(Rybicki & Lightman 1979). Keeping in mind that j_{ν} / ν^2 and $\alpha_{\nu} \nu$ are Lorentz invariant and $\nu' = \nu \gamma (1 - \beta \mu)$, we can write the radiative transfer equation (equation 8) explicitly. We first write an expression for the optical depth to the observer, which will later help us gain some intuition for the results. The optical depth to the observer is given by:

$$\tau(x, y) = \int \alpha_{\nu} ds = \frac{2}{\phi^{5/3}} \int_y^{y_{max}(x)} dy \frac{y^{5/3}}{\chi^{10/9-\delta}(x, y) (1 + 7\chi(x, y)y^4)^{2/3}} , \quad (16)$$

where $\chi(x, y)$ is obtained from equation 13, and $y_{max}(x)$ is obtained by solving $\chi(x, y) = 1$ for y .

We define a ‘‘typical’’ specific intensity I_0 by: $I_0 \equiv S_\nu(y = \chi = 1)$, where the source function S_ν is defined as: $S_\nu \equiv j_\nu/\alpha_\nu$. Expressing I_ν in units of I_0 : $I_\nu \equiv \tilde{I}_\nu I_0$, we write equation 8 in terms of the dimensionless variables \tilde{I}_ν :

$$\frac{d\tilde{I}_\nu}{dy} = \frac{2y^{5/3}}{\phi^{5/3}\chi^{10/9-\delta}(1-7\chi y^4)^{2/3}} \left(\frac{8y\chi^{1/3}}{(1-7\chi y^4)} - \tilde{I}_\nu \right), \quad (17)$$

where we took $ds \cong R_\perp dy$. This equation can be solved numerically for a given magnetic field model and a given value of ϕ , for different values of x , thus obtaining $I_\nu(x)$. The observed flux density is given by:

$$F_\nu(T) \cong \frac{(1+z)}{d_L^2} \int dS_\perp I_\nu = 2\pi(1+z) \left(\frac{R_{\perp,max}(T)}{d_L} \right)^2 \int_0^1 x dx I_\nu(x, T). \quad (18)$$

As can be seen from equation 18, the surface brightness is proportional to I_ν : $dF_\nu/dS_\perp \propto I_\nu$. This means that we also obtain the observed image of a GRB afterglow, by calculating the observed flux density in this way.

4 The Spectra and Observed Image

Solving equations 17 and 18, we calculate the spectra for the three magnetic field models (B , B_{rad} and B_\perp). These spectra are shown in Figure 2. We define the self absorption frequency ν_a as the frequency at which the asymptotic high and low frequency power laws meet. For the equipartition magnetic field model B we obtain:

$$\nu_a = 0.247\nu_0 = 1.05 \times 10^9 (1+z)^{-1} \left(\frac{p+2}{3p+2} \right)^{3/5} \frac{(p-1)^{8/5}}{p-2} \epsilon_e^{-1} \epsilon_B^{1/5} E_{52}^{1/5} n_1^{3/5} \text{Hz}, \quad (19)$$

while for the B_\perp model it is lower by 6% and for the B_{rad} model it is higher by 14%. For $\nu \ll \nu_a$ the system is optically thick, and therefore the radiation reaching an observer is essentially emitted near the edge facing the observer. It reflects the electron distribution there, and it is independent of the magnetic field model. For $\nu > \nu_a$ the system is optically thin and the flux density is different for the various magnetic field models.

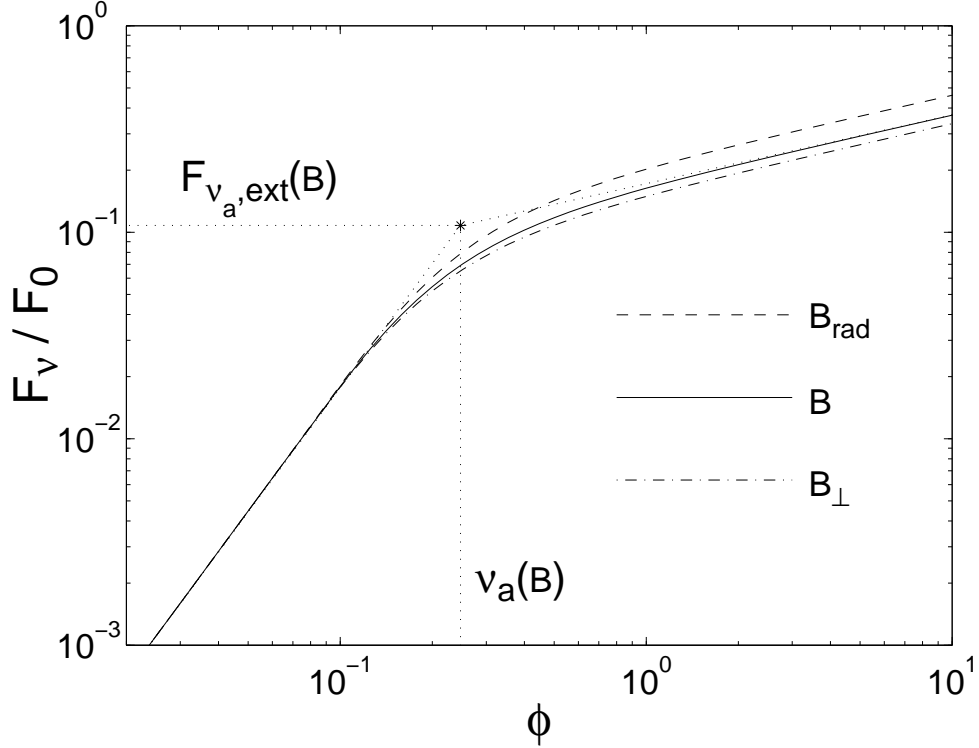


Figure 2: The spectra for different magnetic field models. The frequency ν_a and the flux density $F_{\nu_a,ext}$ are defined at the point where the extrapolations of the power laws meet, as is illustrated for the equipartition magnetic field model B . ν_a is constant in time, $F_{\nu_a,ext} \propto T^{1/2}$ and both don't change significantly between the different magnetic field models. For $\phi \ll 1$ ($\nu \ll \nu_a$) the system is optically thick, and the flux density reflects the electron distribution (or the Lorentz boosted “effective temperature” of the electrons) and is independent of the magnetic field model.

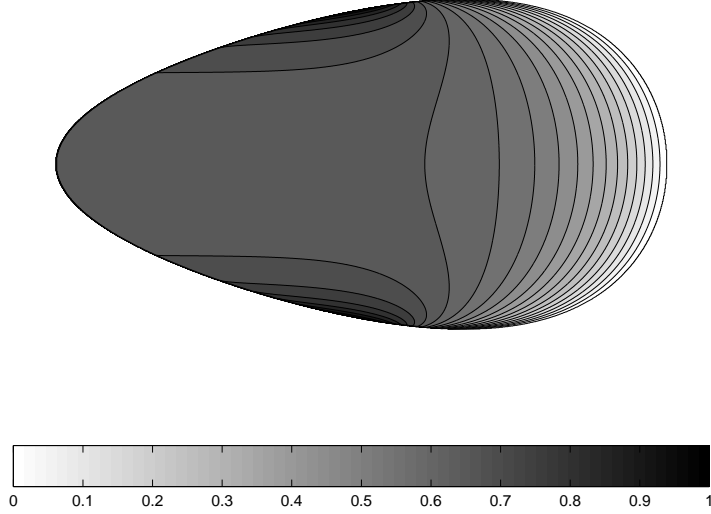


Figure 3: The optical depth τ to the observer, divided by the maximal optical depth ($\tau = \tau_{max} = 1.08 \times (\nu/\nu_a)^{-5/3}$ is black). τ_{max} is obtained at $x \equiv R_{\perp}/R_{\perp,max} = 0.93$. The contour lines are equally spaced with a 5% interval between following contour lines.

The ratio τ/τ_{max} (where τ is the optical depth and τ_{max} is its maximal value) for the equipartition B model is shown in Figure 3. Since $\tau_{\nu} \propto \phi^{-5/3}$ everywhere, τ/τ_{max} is frequency independent. The contour lines of τ_{ν} are dense where the absorption coefficient α_{ν} is large. τ_{max} is obtained at $x \cong 0.93$, i.e. quite close to the edge of the image, since then the whole trajectory to the observer is relatively close to the shock front, implying large values of α_{ν} and a large contribution to τ_{ν} . τ_{max} is a good indicator for the opacity of the system, and for the equipartition B model it is given by: $\tau_{max} = 1.08 \times (\nu/\nu_a)^{-5/3}$.

We define $F_{\nu_a,ext}$ as the extrapolated flux density at ν_a (see Figure 2). For the equipartition B model we obtain:

$$F_{\nu_a,ext} = 0.108F_0 = 142(1+z) \left(\frac{p+2}{3p+2} \right)^{1/5} \frac{(p-1)^{6/5}}{(p-2)} d_{L28}^{-2} \epsilon_e^{-1} \epsilon_B^{2/5} E_{52}^{9/10} n_1^{7/10} T_{days}^{1/2} \mu\text{Jy} , \quad (20)$$

While for the B_{\perp} model it is lower by 12% and for the B_{rad} model it is higher by 23%. The actual flux density at ν_a is around 35% lower than

$F_{\nu_a,ext}$: $F_{\nu_a} \cong 0.65F_{\nu_a,ext}$. The values of $F_{\nu_a,ext}$ and ν_a are useful, since for $\nu \ll \nu_a$ magnitude smaller than ν_a (assuming $\nu_m > \nu_a$) the flux density is given by: $F_\nu \cong F_{\nu_a,ext}(\nu/\nu_a)^2$, and for $\nu_a \ll \nu \ll \nu_m$ it is given by: $F_\nu \cong F_{\nu_a,ext}(\nu/\nu_a)^{1/3}$. Both approximations are already good within a few percent for frequencies a factor ~ 3 below or above ν_a , respectively.

It is interesting to compare the spectra obtained for the BM solution to that obtained for a simplistic model of a static homogeneous disk. This comparison should help us learn whether the fact that the spectra is rounded up near ν_a should be attributed mainly to the specific hydrodynamics used, or whether it is a more general feature of a calculation accounting for self absorption. For a static disk we obtain the well known result:

$$F_\nu = F_{\nu_a,ext}^* \psi^2 \left(1 - \exp[-\psi^{-5/3}]\right) \quad , \quad \psi \equiv \frac{\nu}{\nu_a^*} \quad , \quad (21)$$

where the constants $F_{\nu_a,ext}^*$ and ν_a^* are determined by the radius and width of the disk and by the hydrodynamic parameters of the emitting matter within the disk. If these parameters are set so that the two stated quantities equal those in equations 20 and 19, respectively, the resulting flux density is very similar to that obtained for the BM solution. Substituting equations 20 and 19 into equation 21 can thus serve as a good approximation (better than 3%) for the observed flux density at $\nu \ll \nu_m$. This similarity implies that the shape of the spectrum near ν_a is rather independent of the specific hydrodynamic solution considered. On the other hand, the exact values of ν_a and $F_{\nu_a,ext}$ depend significantly on the hydrodynamics, and can not be determined without the detailed calculation. A simplified calculation for ν_a^* could for example yield ν_0 (equation 5) instead of ν_a that is given in equation 19.

The surface brightness as a function of $x \equiv R_\perp/R_{\perp,max}$ for the equipartition magnetic field model B is shown in Figure 4, for a few representative values of $\phi \equiv \nu/\nu_0$. An illustration of the observed image of a GRB afterglow, which is implied from the surface brightness, is shown in Figure 5. As a reference, the image for $\nu \gg \nu_m$, which was derived in GPS, is also presented.

For $\nu \gg \nu_a$ the system is optically thin and the result coincides with that obtained in GPS for $\nu \ll \nu_m$. There is a bright ring near the outer edge of the image, and the surface brightness at the center of the image is 58% of its average value. As ν decreases, the contrast between the edge and the center of the image decreases and the system becomes increasingly optically thick.

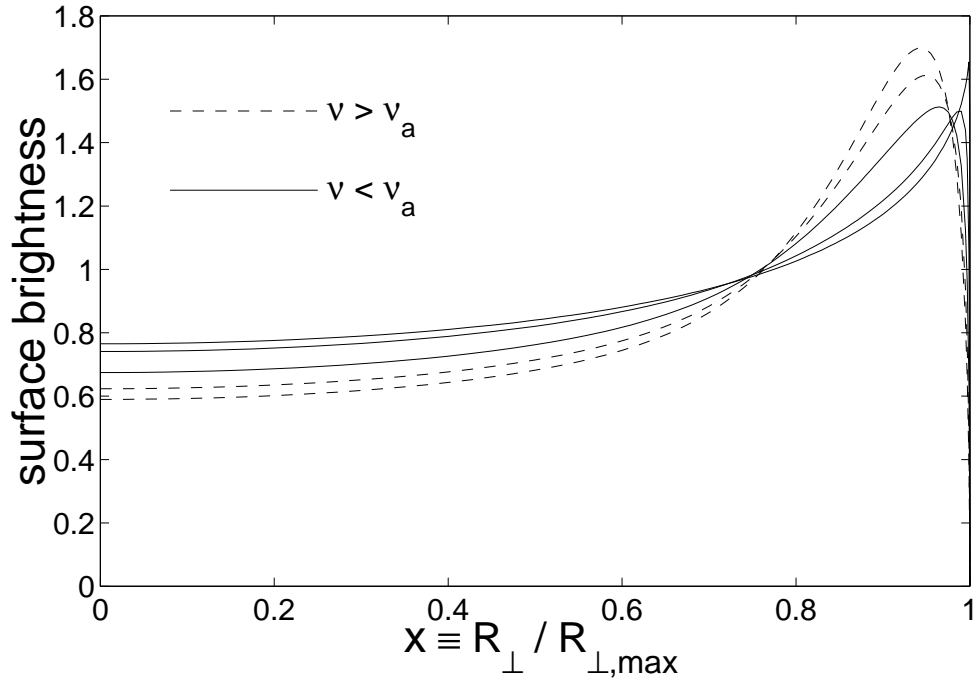


Figure 4: The surface brightness divided by the average surface brightness, as a function of x , for $\text{Log}_{10}(\phi) = -1.5, -1 - 0.75, -0.5, 0$ (corresponding to $\nu/\nu_a = 0.13, 0.40, 0.72, 0.28, 4.05$). At high frequencies the contrast between the center and the edge of the image is larger than at low frequencies. At low frequencies the system is optically thick, and the surface brightness reflects the “effective temperature” of the electrons at the edge of “egg” depicted in Figure 1, on the side facing the observer.

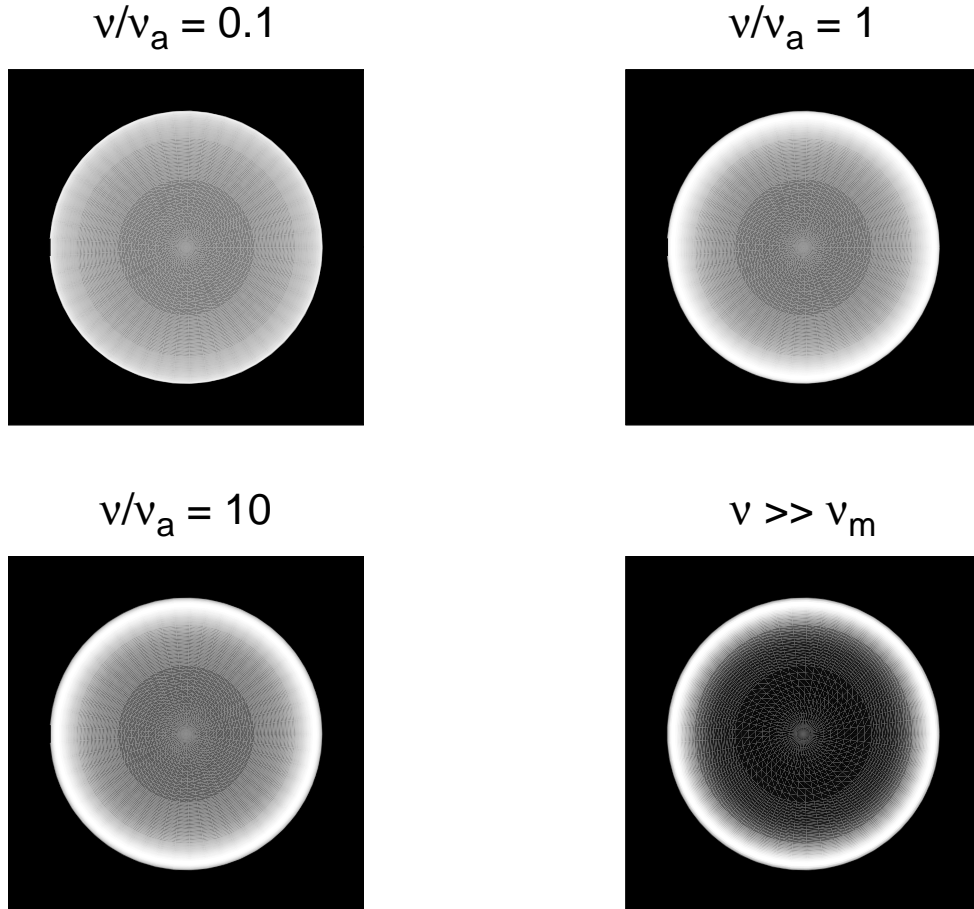


Figure 5: The observed image of a GRB afterglow, at several frequencies. At high frequencies there is a bright ring near the outer edge of the image, and the contrast between the center and the edge of the image is larger than at low frequencies. At low frequencies the surface brightness increases as one moves from the center towards the edge, until it drops very sharply, due to the fact that the system becomes optically thin near the edge. The last image, for $\nu \gg \nu_M$, is taken from GPS and it is brought as a reference, to illustrate the change in the relative surface brightness along the image over a large range of frequencies. At $\nu \gg \nu_m$ there is a thin bright ring at the outer edge of the image, and the surface brightness at the center is only a few percent of its maximal value.

As a result, the surface brightness reflects the Lorentz boosted “effective temperature” of the electron distribution, at the outer edge of the “egg” depicted in Figures 1 and 3, on the side facing the observer. Larger values of x correspond to smaller shock radii R , and since the electrons possess a larger Lorentz factor (i.e. a larger “effective temperature”) at smaller radii, the surface brightness increases with x . This is true as long as the optical depth is still large. Since the length of the trajectory within the system approaches zero as $x \rightarrow 1$, for every given frequency ν the system becomes optically thin for values of x sufficiently close to 1. For frequencies smaller than ν_a by more than one or two orders of magnitude, this occurs at $1 - x \ll 1$ so that the drop in the surface brightness near $x = 1$ is extremely sharp. For $\nu \ll \nu_a$ the surface brightness at the center of the image is 77% of its average value, resulting in an almost uniform disk, rather than a ring which is obtained for $\nu > \nu_a$. The uniformity of the image for $\nu \ll \nu_a$ stands out even more when compared to $\nu \gg \nu_m$, where there is a thin bright ring on the outer edge of the image and the surface brightness at the center is only a few percent of its maximal value.

5 Comparison to Observations

We now fit the theoretical spectra calculated, to the radio frequencies observations of the afterglow of GRB970508 (Fig. 4 of Shepherd 1998). Perhaps a future near enough GRB will result in a sufficient resolution, that will enable us compare the predicted images of a GRB afterglow to observations.

Since both ν_0 and F_0 depend on the parameters of the model (see equations 5 and 7), we have two degrees of freedom in trying to fit the calculated spectra to the observed data. We fit the equipartition magnetic field model B to the data in Shepherd et al (1998), and obtain:

$$\nu_a = 3.1 \pm 0.4 \times 10^9 \text{Hz} \quad , \quad F_{\nu_a, \text{ext}} = 450 \pm 37 \mu\text{Jy} \quad , \quad (22)$$

with $\chi^2/\text{dof} = 0.48$. The fit is presented in Figure 6.

The errors quoted are statistical errors. The actual errors are probably larger due to uncertainty in the radio flux due to scintillation, and due to the fact that not all the observations are exactly simultaneous (see Shepherd 1998).

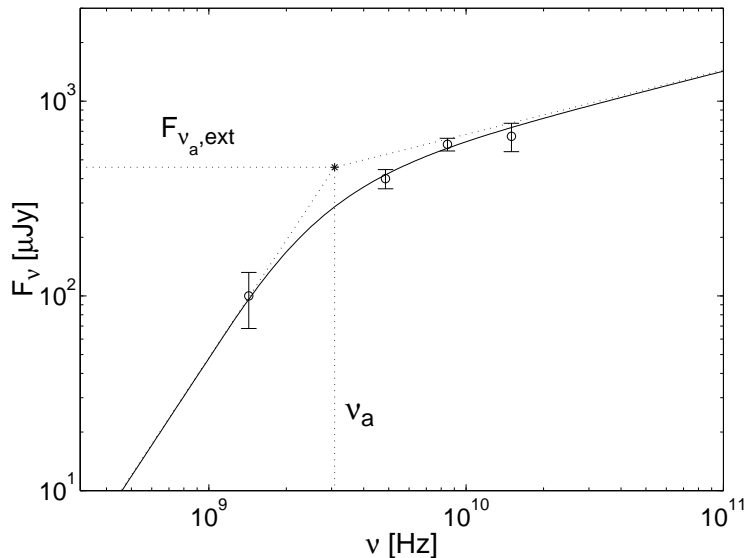


Figure 6: A fit of the calculated spectra, to radio observations of the afterglow of GRB970508. We obtained: $\nu_a = 3.1 \pm 0.4 \times 10^9 \text{Hz}$ and $F_{\nu_a,ext} = 450 \pm 37 \mu\text{Jy}$.

Substituting these results in equations 19 and 20, respectively, we obtain two constraints on the physical parameters of the burst. The luminosity distance depends on the cosmological model. For $\Omega = 1$, $\Lambda = 0$ (which implies: $d_L = 2(1+z - \sqrt{1+z})c/H_0$), $H_0 = 65 \text{Kms}^{-1}\text{Mpc}^{-1}$ and $z = 0.835$ we find:

$$\frac{(p-1)^{8/5}}{(p-2)} \left(\frac{p+2}{3p+2} \right)^{3/5} \epsilon_e^{-1} \epsilon_B^{1/5} E_{52}^{1/5} n_1^{3/5} = 5.43, \quad (23)$$

$$\frac{(p-1)^{6/5}}{(p-2)} \left(\frac{p+2}{3p+2} \right)^{1/5} \epsilon_e^{-1} \epsilon_B^{2/5} E_{52}^{9/10} n_1^{7/10} = 1.22. \quad (24)$$

Substitution of the value for ν_a from the data (equation 22) into equation 19, yields an equation different by a factor of ~ 2 from equation 22 of Wijers & Galama (1998). The difference is mainly due to a different theoretical value they used for ν_a . They also used a slightly different value of ν_a as corresponding to the same observational data. This factor of ~ 2 implies significant corrections to the values of the physical parameters of the burst

TABLE 1

Estimates of the Physical Parameters of GRB970508.

model	broken power law	modified ν_a	modified $\nu_a, \nu_m, F_{\nu_m}, \nu_c$
E_{52}	3.7	2	0.53
ϵ_e	0.13	0.24	0.57
ϵ_B	0.068	0.011	0.0082
n_1	0.035	0.70	5.3

Table 1: The first row depicts the values of the physical parameters of GRB970508 as calculated by Wijers & Galama (1998). The other rows show how these values change when some of the equations they used in the calculation are corrected. The first line lists the measurable quantities, whose equations were altered.

(see the second row of Table 1). For example, n_1 (or n in their notation) becomes a factor of ~ 20 larger: $n_1 = 0.7$ instead of $n_1 = 0.035$.

We modify the estimates further using more detailed calculations of the spectrum near the peak flux (GPS), and use a different estimate for the cooling frequency ν_c (Sari, Piran & Narayan 1998). We discover that the values obtained for the physical parameters of a burst are very sensitive to the theoretical model of the spectrum. In order to illustrate this we show in Table 1 the physical parameters of GRB970508 for different estimates of the spectrum. The first column uses a broken power law spectrum (Wijers & Galama 1998); the second column uses a corrected theoretical value for ν_a from equation 19 and a corrected observational value for ν_a from equation 22; the third column adds a modified theoretical values to ν_m and F_{ν_m} (which are taken from GPS - denoted there as ν_{peak} and $F_{\nu,max}$) and a different estimate for the cooling frequency ν_c (from Sari, Piran & Narayan 1998), keeping the observational values from Wijers & Galama (1998).

Our best values (with all modifications added) are $E_{52} = 0.53$, $\epsilon_e = 0.57$, $\epsilon_B = 0.0082$ and $n_1 = 5.3$. These values differ by one to two orders of magnitude than the values obtained by Wijers & Galama (1998) using a

broken power law spectra. One must keep in mind that it is difficult to obtain an accurate estimate of the various observables from the observed data. It is especially difficult to determine ν_m , F_{ν_m} and ν_c . Therefore, more than obtaining a better estimate of the physical parameters of the burst, these calculations show the sensitivity of this method and the need for more accurate data.

Sufficient observational data has been gathered on the radio afterglow of GRB980329, to enable a fit similar to the one we made for GRB970508. Such a fit was carried out by Taylor et al (1998). The theoretical formula for the flux density that was used for the fit is identical to equation 21. Since this is a good approximation for the shape of the spectra near ν_a , we can use the values extracted from the data to obtain constraints on the physical parameters of GRB980329.

The values used by Taylor et al for the flux density are mean values over the first month. Since $F_{\nu_a} \propto T^{1/2}$, this corresponds to the flux density at ~ 15 days. The values extracted from the data are:

$$\nu_a \cong 1.3 \times 10^{10} \text{Hz} \quad , \quad F_{\nu_a, \text{ext}} \cong 600 \mu\text{Jy} \quad . \quad (25)$$

Substituting these results in equations 19 and 20, respectively, we obtain two constraints on the parameters of GRB980329. For $\Omega = 1$, $\Lambda = 0$ and $H_0 = 65 \text{Kms}^{-1} \text{Mpc}^{-1}$ we find:

$$\frac{2}{(1+z)} \frac{(p-1)^{8/5}}{(p-2)} \left(\frac{p+2}{3p+2} \right)^{3/5} \epsilon_e^{-1} \epsilon_B^{1/5} E_{52}^{1/5} n_1^{3/5} \cong 26 \quad , \quad (26)$$

$$\left(\frac{\sqrt{2}-1}{\sqrt{1+z}-1} \right)^2 \frac{(p-1)^{6/5}}{(p-2)} \left(\frac{p+2}{3p+2} \right)^{1/5} \epsilon_e^{-1} \epsilon_B^{2/5} E_{52}^{9/10} n_1^{7/10} \cong 1.5 \quad , \quad (27)$$

where the red shift z of this burst is not yet known.

6 Discussion

We have considered synchrotron emission from a system moving relativistically, taking into account the effect of synchrotron self absorption. We have assumed an adiabatic evolution and used the self similar solution of Blandford & McKee (1976) to describe the matter behind the shock. This solution describes an extreme relativistic spherical blast wave expanding into a cold

uniform medium. Our calculations accounted for the emission from the whole region behind the shock front.

We have assumed a power law distribution of electrons with an isotropic velocity distribution. Three alternative models have been considered for the evolution of the magnetic field, including an equipartition model. We have calculated the flux density at frequencies near the self absorption frequency ν_a , under the assumption that $\nu_a \ll \nu_m$.

We have obtained an expression for the self absorption frequency ν_a , which we defined as the frequency at the point where the extrapolations of the asymptotic power laws above and below the ν_a meet. The value we obtained for ν_a is close to the value obtained by Wijers & Galama (1998), and a factor of ~ 4 for $p = 2.5$ (or a factor of ~ 7 for $p = 2.2$) larger than the value obtained by Waxman (1997b).

We have calculated the observed spectra near ν_a for three different magnetic field models (Figure 4). The spectra differs more than a few percent from the asymptotic power laws only for frequencies less than half an order of magnitude above or below ν_a . This applies to all the magnetic field models we have considered.

Together with the afterglow images obtained in GPS we now have a complete set of the observed image over a wide range of frequencies (see Figures 4 and 5). For $\nu \gg \nu_m$ there is a thin bright ring on the outer edge of the image, and the surface brightness at the center of the image is only a few percent of its maximal value. For $\nu_a \ll \nu < \nu_m$ there is a wider ring and the contrast between the center and the edge of the image is smaller, with 58% of the average surface brightness at the center. For $\nu \ll \nu_a$ the image is even more homogeneous, with 77% of the average surface brightness at the center.

The observed image in the radio frequencies is of special importance, since the best resolution is obtained in radio, with VLBI. A sufficient resolution could be reached with a nearby GRB ($z \sim 0.2$) to resolve the inner structure of the image in radio frequencies.

We have fitted the theoretical spectra to observational data of the afterglow of GRB970508 (Shepherd 1998) and extracted the values of ν_a and $F_{\nu_a,ext}$ from the data (equation 22). Substituting these values into the theoretical expressions we obtained two equations for the physical parameters. The behavior of the spectra near ν_m can supply two other equations, namely the equations for the peak frequency and for the peak flux (adding only one independent equation to the two equations for ν_a and $F_{\nu_a,ext}$). An additional

independent equation is obtained for ν_c . The power law p of the electron distribution can be determined from the high energy slope ($\nu \gg \nu_m$). It is therefore possible with sufficient observational data to determine all the physical parameters of the afterglow: p , ϵ_e , ϵ_B , E_{52} and n_1 . A similar calculation (using an equation for the cooling frequency ν_c instead of $F_{\nu_a,ext}$) was made by Wijers & Galama (1998) for GRB970508. In fact combining this equation we could even have an over-constrained system and check for consistency of the solution. The equation we obtained from ν_a differs by a factor of ~ 2 from the corresponding equation given in Wijers & Galama. This has a significant effect (up to a factor of ~ 20) on the values of the physical parameters of the burst which they have given. We have shown (Table 1) that if other equations are corrected as well, the values of the physical parameters vary even more (up to two orders of magnitude).

We thank Ehud Cohen for useful discussions and Dale Frail and Shri Kulkarni for observational information. This research was supported by NASA Grant NAG5-3516, and a US-Israel Grant 95-328. Re'em Sari thanks The Clore Foundation for support.

References

- [1] Blandford, R. D. & McKee, C. F. 1976, *Phys. of fluids*, **19**, 1130.
- [2] Granot, J., Piran, T. & Sari, R. 1998. astro-ph/9806192.
- [3] Gruzinov, A. & Waxman, E. 1998. astro-ph/9807111.
- [4] Katz, J. 1994, *ApJ*, **422**, 248.
- [5] Katz, J. & Piran, T. 1997, *ApJ*, **490**, 772.
- [6] Kobayashi, S., Piran, T. & Sari, R. 1998. astro-ph/9803217.
- [7] Panaitescu, A. & Mészáros, P. 1998, *ApJ*, **493**, L31.
- [8] Rybicki, G.B. & Lightman, A.P. 1979, *Radiative Processes in Astrophysics*, Wiley-Interscience.

- [9] Sari, R. 1997, ApJ, **489**, L37
- [10] Sari, R. 1998, ApJ, **494**, L49
- [11] Sari, R., Piran, T. & Narayan, R. 1998, ApJ, **497**, L17.
- [12] Shepherd, D.S., et al. 1998, ApJ, **497**, 859.
- [13] Taylor, D.A., et al. 1998, ApJ, **502**, L115.
- [14] Waxman, E. 1997a, ApJ, **485**, L5.
- [15] Waxman, E. 1997b, ApJ, **489**, L33.
- [16] Waxman, E. 1997c, ApJ, **491**, L19.
- [17] Wijers, R.A.M.J. & Galama, T.J. 1998, astro-ph/9805341.
- [18] Wijers, R.A.M.J., Rees, M.J. & Mészáros, P. 1997, MNRAS, **228**, L51.